Soft-lubrication effect on the lateral migration of a slightly deformed bubble rising near a vertical plane wall

Kazuyasu Sugiyama[1] and Fumio Takemura[2,1]

[1] *Department of Mechanical Engineering, School of Engineering, The University of Tokyo, 7-3-1 Hongo, Bunkyo-ku, Tokyo 113-8656, Japan*
[2] *National Institute of Advanced Industrial Science and Technology, 1-2-1 Namiki, Tsukuba, Ibaraki 305-8564, Japan*

(Dated: November 21, 2008)

Deformation-induced lateral migration of a bubble slowly rising near a vertical plane wall in a stagnant liquid is numerically and theoretically investigated. In particular, our focus is set on a situation with a small clearance c between the bubble interface and the wall. Motivated by the fact that experimentally measured migration velocity (Takemura et al. (2002, J. Fluid Mech. **461**, 277)) is higher than the velocity estimated by the available analytical solution (Magnaudet et al. (2003, J. Fluid Mech. **476**, 115)) using the Faxén mirror image technique for $\kappa(= a/(a+c)) \ll 1$ (here a is the bubble radius), when the clearance parameter $\varepsilon(= c/a)$ is comparable to or smaller than unit, the numerical analysis based on the boundary-fitted finite-difference approach by solving the Stokes equation is performed to complement the experiment. To improve the understandings of a role of the squeezing flow within the bubble-wall gap, the theoretical analysis based on a soft-lubrication approach (Skotheim & Mahadevan (2004, Phys. Rev. Lett. **92**, 245509)) is also performed. The present analyses demonstrate the migration velocity scales $\propto$ Ca $\varepsilon^{-1} V_{B1}$ (here, V_{B1} and Ca denote the rising velocity and the capillary number, respectively) in the limit of $\varepsilon \to 0$.

PACS numbers: 47.55.D-, 47.15.G-, 47.15.gm, 47.11.Bc

Recent technical progress in generating microbubbles [1], including potentials as actuator and sensor, has enhanced the range of applications, e.g., additives to reduce a turbulence friction [2], drug delivery capsules [3], and contrast agents [4]. In many situations, a bubble encounters a boundary wall during its transport process, and a hydrodynamic interaction occurs as characterized by the inter-scale between the bubble and the wall. In practice, it is of primary importance that the bubble undergoes a repulsive or attractive force in the wall-normal direction, which causes a migration [5] and determines the bubble distribution, when translating parallel to the wall. As the simplest model system, one may raise a problem of a spherical bubble rising near a vertical infinite plane wall in a creeping (Stokes) flow. However, there is no mechanism to generate the migration force, as ensured kinematic reversibility by symmetry of the boundary and by linearity in the Stokes equation. In fact, the migration force stems from nonlinearities in the advective momentum transport [6, 7] and the interfacial deformability [7, 8], to break the symmetry. The theoretical success in solving the nontrivial problem of the deformation-induced migration of a bubble or drop was recently made by Magnaudet et al. [7] using the Faxén mirror image technique. However, more recently, an experiment [9] and a numerical simulation [10] indicated that the theory [7] involves something imperfect since it considerably underestimates the migration velocity, despite of consistencies in terms of the buoyant velocity and the deformation. As the most crucial restriction in the theory [7], we raise an assumption in the mirror image technique that the bubble-wall distance is much longer than the bubble radius. In this Letter, to release the constraint of the sufficiently wide bubble-wall distance, performing experimental and theoretical studies, we examine the effect of the distance on the bubble migration.

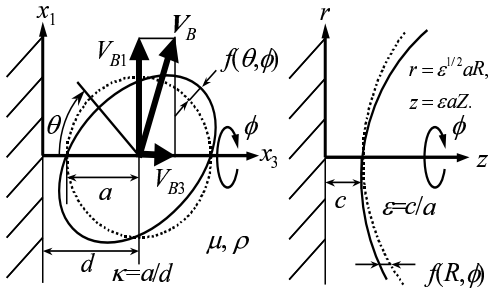

FIG. 1: Schematic of a buoyant bubble moving near a vertical plane wall. The solid outline shows a deformed interface with a deflection f from a spherical interface indicated by the dotted outline. (a) left panel: coordinates system around the bubble. For a bubble radius a and a distance d between the bubble centroid and the wall, the geometry is characterized by $\kappa(= a/d)$, which is assumed to be sufficiently smaller than unit in the analysis of Ref. [7]. (b) right panel: inter-scale coordinates between the bubble surface and the wall and scaling relations suitable to a lubrication theory. A clearance parameter is defined as $\varepsilon = d/a - 1$.

As schematically illustrated in Fig. 1(a), we deal with the migration velocity $V_{B3}(= \boldsymbol{V}_B \cdot \boldsymbol{e}_3)$ of a bubble rising near a vertical plane wall at a distance d between the bubble centroid and the wall. The bubble has an equivalent radius a to that of a sphere with the same volume. The bubble-wall clearance is given by $c = d - a$.

The experimental results used here were measured under the condition that the Reynolds number $2\rho a V_{B1}/\mu$ (here $V_{B1}(=\boldsymbol{V}_B\cdot\boldsymbol{e}_1)$, ρ, and μ respectively denote the rising velocity, the density, and the dynamic viscosity of liquid) is unit or less [9]. The pure lateral migration velocities induced by the deformation V_{B3} were calculated from them by substituting the velocities induced by the inertia effects. We also estimated the interfacial deflection $f(\theta,\phi)$ from the sphere by taking the circumference of the bubble on the plane $x_2=0$. According to the Stokes flow theory for the deformation-induced migration [7], the problem is characterized by two parameters, i.e., an inverse distance $\kappa(=a/d)$ (or a dimensionless clearance $\varepsilon=d/a-1$) and a capillary number $\mathrm{Ca}=\mu V_{B1}/\gamma$ (or a Bond number $\mathrm{Bo}=\rho a^2 g/\gamma$ as used in Ref. [7]). Here γ and g respectively denote the surface tension and the acceleration of gravity. Further, as far as $\mathrm{Ca}\ll 1$, we may use Ca as a perturbation parameter, and reduce the Ca dependence in the problem into that V_{B1}, V_{B3}/Ca and f/Ca are dependent only upon κ or ε. Figure 2 shows the migration velocity V_{B3} away from the wall normalized by $\mathrm{Ca}V_{B1}$ as a function of κ. The measured velocity is found to be much larger than the analytical solution especially for the large κ, where the theoretical assumption $\kappa\ll 1$ is no longer justified. Such an underestimation of the theoretical migration velocity supports the indication in the boundary element simulation carefully dealing with a drop motion in a shear flow [10]. The result implies that there exists an additional ingredient to generate repulsive force for narrow bubble-wall gap, which is not covered by the theory [7].

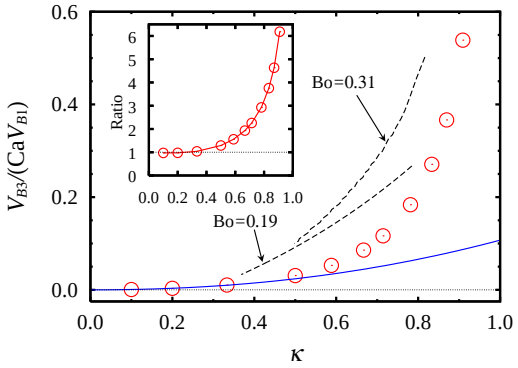

FIG. 2: Migration velocity V_{B3} versus κ. The solid curve indicates the analytical solution [7] $V_{B3}/(\mathrm{Ca}V_{B1})=\frac{3\kappa^2(1+3\kappa/2)}{40(1+3\kappa/4)}$ with the assumption of the sufficiently large distance between the bubble centroid and the wall, i.e., $\kappa\ll 1$. The dashed curve indicates the experimental results [9], and the circle the results obtained by the finite difference simulation discretized in the bipolar coordinates system. The inset shows the simulation result normalized by the analytical solution.

To clarify the physical mechanism of the repulsive force, we numerically address the bubble migration problem. We suppose that the bubble quasi-steadily rises near an infinite flat plate in an stagnant incompressible liquid, and both the Reynolds and capillary numbers are sufficiently smaller than unit. Hence, the problem is well described by the steady Stokes equation for a solenoidal velocity vector and a Laplace law responsible for the bubble deformation. Free-slip and kinetic boundary conditions are imposed on the bubble surface, and a no-slip one on the plane wall. The basic equations are numerically solved by the second-order finite-difference scheme discretized on the bipolar coordinates grid, which is boundary-fitted on both the bubble surface and the wall. Evaluating exact values of the control volume and the cell interfacial area, we take care of the mass and momentum conservations in a discretized form. In a similar manner to Ref. [7], instead of directly solving the flow field with the deformed bubble, we employ the Lorenz reciprocal theorem to determine the migration force and velocity by coupling two flow fields around a spherical bubble translating parallel and perpendicular to the wall. To make sure of the numerical stability and accuracy, we set the clearance parameter in a range of $0.1\le\varepsilon\le 9$.

As shown in the inset of Fig. 2, the ratio of the migration velocity becomes close to unit as κ approaches 0, indicating the simulation captures the analytical solution for small κ [7]. On the other hand, the migration velocity for the bubble closer to the wall (i.e., for larger κ), the discrepancy from the theory is larger. Compared with the experiment, the simulation results reveal low velocity since it cannot capture unknown factors such as small but finite Reynolds number effect, unsteadiness, and measurement uncertainty, which may be inevitably involved in the experiment. Nevertheless, the simulation result also indicates the presence of the additional narrow-gap repulsive force.

To demonstrate the narrow gap effect, we investigate the near-wall deformation, which causes a change in the boundary shape. Introducing an interfacial deflection $f(\theta,\phi)(=\mathrm{Ca}\,a\hat{f}^{(\mathrm{Ca})}(\theta)\cos\phi)$, we write the distance from the bubble centroid to the interface as $a+f$. Figure 3 shows the angular profile of the scaled deflection $-\hat{f}^{(\mathrm{Ca})}/\kappa^2$. Following the analytical solution for $\kappa\ll 1$ [7], it is uniquely arranged as $\frac{3}{4}\sin\theta\cos\theta$. In Fig. 3(a), the present simulation captures the measured deflection. In Fig. 3(b), the simulation result for the wide bubble-wall gap ($\varepsilon=4$) is in agreement with the theory [7]. Note that the agreement is confirmed to be better in the wider separation. On the other hand, for the narrower gap ($\varepsilon=0.1,\ 0.5,\ 0.6$), the discrepancy from the theory is considerably larger especially in the wall neighbor ($\theta\sim 0$), that may be related to the larger discrepancy in the migration velocity as shown in Fig. 2. Namely, it indicates that for small ε, the bubble deformation is preferentially enhanced within the narrow bubble-wall gap, and its squeezing effect promotes the bubble migration.

To shed more light on the role of the inter-scale hydro-

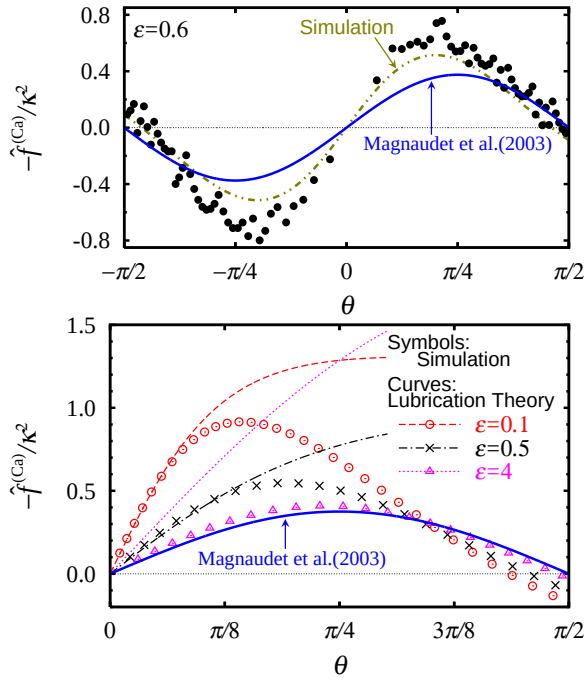

FIG. 3: Angular profile of the scaled deflection. The solid curve indicates the analytical solution [7], $-\hat{f}^{(\mathrm{Ca})}/\kappa^2 = \frac{3}{4}\sin\theta\cos\theta$, with the assumption of $\kappa \ll 1$. (a) upper panel: comparison between the experiment [9] (symbols, $Ca = 0.080$) and simulation. (b) lower panel: comparison between the present simulation, indicated by the symbols, and soft-lubrication theory (12) $-\hat{f}^{(\mathrm{Ca})}/\kappa^2 = \frac{3}{5\kappa^2\sin\theta}\log(1+\frac{\sin^2\theta}{2\varepsilon})$, by the dashed, dotted, and dashed-dotted curves.

dynamics, a lubrication analysis is performed. It should be noted that one can access a relevant physical picture, so-called 'soft-lubrication' problem, recently addressed by Skotheim & Mahadevan [11], who derived the elastic deformation generating the lift force. We prescribe the wall-parallel velocity V_{B1} for ease in completing the analysis, and employ standard lubrication assumption, i.e., $\varepsilon \ll 1$. We also suppose small capillary number $\mathrm{Ca} \ll 1$ resulting in the small deformation. Further, to make sure of the inclination of the near-wall interface to the plane wall to be sufficiently small, we adopt an additional constraint $\varepsilon^{-3/2}\mathrm{Ca} \ll 1$. For the coordinates as illustrated in Fig. 1(b) (see e.g. Ref. [12]), $Z = H(R) = 1 + R^2/2$ represents the interface within a portion $R \sim O(1)$, if the deformation is absent. Using ε and Ca, we write the velocity vector, the pressure, and the deflection f of the interface in an expansion form

$$\frac{u_r(r,\phi,z)}{V_{B1}} = \hat{U}_r^{(0)}(R,Z)\cos\phi + \varepsilon^{-3/2}\mathrm{Ca}\hat{U}_r^{(f)}(R,Z) + ..., \tag{1}$$

$$\frac{u_\phi(r,\phi,z)}{V_{B1}} = \hat{U}_\phi^{(0)}(R,Z)\sin\phi + ..., \tag{2}$$

$$\frac{u_z(r,\phi,z)}{V_{B1}} = \varepsilon^{1/2}\hat{U}_z^{(0)}(R,Z)\cos\phi + \varepsilon^{-1}\mathrm{Ca}\hat{U}_z^{(f)}(R,Z) + ..., \tag{3}$$

$$\frac{ap(r,\phi,z)}{\mu V_{B1}} = \varepsilon^{-3/2}\hat{P}^{(0)}(R)\cos\phi + \varepsilon^{-3}\mathrm{Ca}\hat{P}^{(f)}(R) + ..., \tag{4}$$

$$f(r,\phi) = \varepsilon^{-1/2}\mathrm{Ca}\hat{F}(R)\cos\phi, \tag{5}$$

whose scaling relations are suitable to all equations to appear afterward. Following the spirit of the lubrication theory, we solve the governing equations

$$\frac{1}{R}\frac{\partial(Ru_r)}{\partial R} + \frac{1}{R}\frac{\partial u_\phi}{\partial\phi} + \varepsilon^{-1/2}\frac{\partial u_z}{\partial Z} = 0, \tag{6}$$

$$-\frac{\partial p}{\partial R} + \varepsilon^{-3/2}\frac{\partial^2 u_r}{\partial Z^2} = -\frac{1}{R}\frac{\partial p}{\partial\phi} + \varepsilon^{-3/2}\frac{\partial^2 u_\phi}{\partial Z^2} = -\frac{\partial p}{\partial Z} = 0, \tag{7}$$

with the kinetic condition

$$\begin{aligned} &R\hat{U}_r^{(0)} - \hat{U}_z^{(0)} - R \\ &= R\hat{U}_r^{(f)} - \hat{U}_z^{(f)} - \frac{1}{2}\frac{\partial\hat{F}}{\partial R}\hat{U}_r^{(0)} + \frac{\hat{F}}{2R}\hat{U}_\phi^{(0)} - \frac{\hat{F}R}{2}\frac{\partial\hat{U}_r^{(0)}}{\partial Z} \\ &+ \frac{\hat{F}}{2}\frac{\partial\hat{U}_z^{(0)}}{\partial Z} + \frac{1}{2}\left(\frac{\partial\hat{F}}{\partial R} + \frac{\hat{F}}{R}\right) = 0 \quad \text{at} \quad Z = H, \end{aligned} \tag{8, 9}$$

the free-slip boundary conditions

$$\frac{\partial\hat{U}_r^{(0)}}{\partial Z} = \frac{\partial\hat{U}_\phi^{(0)}}{\partial Z} = \frac{\partial\hat{U}_r^{(f)}}{\partial Z} - \frac{\hat{F}}{2}\frac{\partial^2\hat{U}_r^{(0)}}{\partial Z^2} = 0 \quad \text{at} \quad Z = H, \tag{10}$$

and the no-slip boundary condition $\boldsymbol{u} = 0$ on the plane wall $Z = 0$. Considering that the drag force acting on the bubble is deduced $O(\log\varepsilon)$ from the earlier analysis for a motion of a rigid sphere [12], and the normal stress on the bubble surface is dominated by the pressure $p \sim O(\varepsilon^{-3/2})$ as compared with $\partial_r u_r \sim O(\varepsilon^{-1/2})$, $u_r/r \sim O(\varepsilon^{-1/2})$, $u_\phi/r \sim O(\varepsilon^{-1/2})$, and $\partial_z u_z \sim O(\varepsilon^{-1/2})$, which are related to the viscous stresses, simplifies the Laplace law into

$$\frac{\partial}{\partial R}\left(\frac{1}{R}\frac{\partial(R\hat{F})}{\partial R}\right) = \hat{P}^{(0)}. \tag{11}$$

We obtain the leading-order pressure and interfacial deflection

$$\hat{P}^{(0)} = \frac{3R}{5H^2}, \quad \hat{F} = -\frac{3\log H}{5R}. \tag{12}$$

To ensure the appearance of the soft-lubrication effect, Fig. 3(b) shows the deflection based on (12), which is in agreement with the simulation results for the narrow gap ($\varepsilon = 0.1$, 0.5) in the region of the small $\theta(\approx \varepsilon^{1/2}R)$,

indicating the neighborhood of the wall. Therefore, the present theory is responsible for the discrepancy of the narrow gap experiment and simulation from the available theory [7]. Note that for small ε, we confirm that the pressure profile for small θ is also consistent with (12). From (6), (7) and the no-slip condition at $Z = 0$, we write the higher-order quantities as

$$\hat{U}_r^{(f)}(R,Z) = A_2(R)Z^2 + A_1(R)Z, \tag{13}$$

$$\hat{U}_z^{(f)}(R,Z) = -\frac{1}{3R}\frac{\mathrm{d}(RA_2)}{\mathrm{d}R}Z^3 - \frac{1}{2R}\frac{\mathrm{d}(RA_1)}{\mathrm{d}R}Z^2, \tag{14}$$

$$\hat{P}^{(f)}(R) = \int_\infty^R \mathrm{d}\bar{R}\; 2A_2(\bar{R}), \tag{15}$$

which quantify the deformation-induced migration force. The R dependent functions A_1 and A_2 are determined from (9) and (10). Using a solution $A_2 = -9(4 - R^2)\log H/(50H^4R)$, we obtain the lateral force F_M to cancel the migration velocity and to maintain the wall-parallel motion

$$\begin{aligned} F_M \to \lim_{R\to\infty} \mu a V_{B1} \int_0^{2\pi}\mathrm{d}\phi \int_0^R \mathrm{d}(\varepsilon^{1/2}\bar{R})\; \varepsilon^{1/2}\bar{R}\; \varepsilon^{-3}\mathrm{Ca}\hat{P}^{(f)}(\bar{R}) \\ = \frac{3\pi\mu a \mathrm{Ca} V_{B1}}{50}\varepsilon^{-2} \quad \text{as} \quad \varepsilon \to 0. \end{aligned} \tag{16}$$

From Bart [13], the drag force acting on the bubble translating perpendicular to the plane wall at unit speed is $F_{DC} \to 3\pi\mu a/(2\varepsilon)$ as $\varepsilon \to 0$. Thus, the migration velocity asymptotically obeys

$$V_{B3} = \frac{F_M}{F_{DC}} \to \frac{\mathrm{Ca}V_{B1}}{25}\varepsilon^{-1} \quad \text{as} \quad \varepsilon \to 0. \tag{17}$$

To validate the asymptotic solutions, Fig. 4 and the inset show the scaled migration velocity and force, respectively, as a function of the clearance parameter ε. The simulation results are consistent with two asymptotic behaviors based on the soft-lubrication theory for $\varepsilon \ll 1$ as well as the mirror image technique for $\varepsilon \gg 1$. The theories provide the different exponents of the migration velocity scaling with respect to ε, namely it scales $V_{B3}/V_{B1} \propto \mathrm{Ca}\,\varepsilon^{-2}$ for $\varepsilon \gg 1$ and $V_{B3}/V_{B1} \propto \mathrm{Ca}\,\varepsilon^{-1}$ for $\varepsilon \ll 1$. The latter scaling relation is found in this Letter.

In conclusion, we demonstrated that the former theory [7] is valid to describe the deformation-induced lift force as far as the gap between the bubble and the wall is sufficiently wide ($\kappa \ll 1$). On the other hand, for the narrow gap case with the clearance parameter ε smaller than unit, the soft-lubrication effect crucially appears to induce the migration velocity asymptotically scalingwise $V_{B3} \propto \mathrm{Ca}\,\varepsilon^{-1}V_{B1}$.

We thank Shu Takagi for many fruitful discussions.

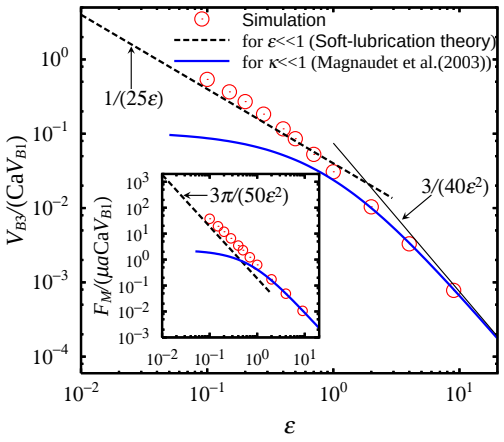

FIG. 4: The migration velocity versus the clearance parameter ε. The circle indicates the results obtained by the present finite difference simulation discretized in the bipolar coordinates system. The solid, and dashed curves correspond to the analytical solution $V_{B3} = \frac{3}{40}\mathrm{Ca}V_{B1}\kappa^2\frac{1+3\kappa/2}{1+3\kappa/4}$ [7], and $V_{B3} = \frac{1}{25}\mathrm{Ca}V_{B1}\varepsilon^{-1}$ derived by means of the soft-lubrication technique [11], respectively. The inset shows the migration force.

[1] e.g., T. Makuta, F. Takemura, E. Hihara, Y. Matsumoto and M. Shoji, J. Fluid Mech. **548**, 113 (2006); P. Garstecki, M.J. Fuerstman, H.A. Stone and G.M. Whitesides, Lab Chip **6**, 437 (2006).

[2] A. Serizawa, T. Inui, T. Yahiro and Z. Kawahara, Multiphase Sci. and Tech. **17**, 79 (2005).

[3] M.J. Shortencarier, P.A. Dayton, S.H. Bloch, P.A. Schumann, T.O. Matsunaga and K.W. Ferrara, IEEE Trans. Ultrason. Ferroelectr. Freq. Control **51**, 821 (2004).

[4] J.-M. Correas, L. Bridal, A. Lesavre, A. Méjean, M. Claudon and O. Hélénon, Eur. Radiol. **11**, 1316 (2001).

[5] T. Hibiki and M. Ishii, Chem. Eng. Sci. **62**, 6457 (2007).

[6] P. Vasseur and R.G. Cox, J. Fluid Mech. **78** 385 (1976); P. Vasseur and R.G. Cox, J. Fluid Mech. **80** 561 (1977); P. Cherukat and J.B. McLaughlin, J. Fluid Mech. **263**, 1 (1994).

[7] J. Magnaudet, S. Takagi and D. Legendre, J. Fluid Mech. **476**, 115 (2003).

[8] B.P. Ho and L.G. Leal, J. Fluid Mech. **76**, 783 (1976); P.C.-H. Chan and L.G. Leal, J. Fluid Mech. **92**, 131 (1979).

[9] F. Takemura, S. Takagi, J. Magnaudet and Y. Matsumoto, J. Fluid Mech. **461**, 277 (2002).

[10] Y. Wang and P. Dimitrakopoulos, Phys. Fluids **18**, 082106 (2006).

[11] J.M. Skotheim and L. Mahadevan, Phys. Rev. Lett. **92**, 245509 (2004); J.M. Skotheim and L. Mahadevan, Phys. Fluids **17**, 092101 (2005);

[12] M.E. O'Neill and K. Stewartson, J. Fluid Mech. **14**, 170 (1967).

[13] E. Bart, Chem. Eng. Sci. **23**, 193 (1968).